Journal of Neuroscience Methods 430 (2026) 110725

Contents lists available at ScienceDirect

Journal of Neuroscience Methods

journal homepage: www.elsevier.com/locate/jneumeth

Refined affinity purification protocol for CAMs using minimal mouse brain material

Agathe Henocq [a], Wouter Doff [b], Dick Dekkers [b], Geeske M. van Woerden [c,d], Jeroen A.A. Demmers [b], Dimphna H. Meijer [a,*]

[a] Department of Bionanoscience, Kavli Institute of Nanoscience Delft, Delft University of Technology, van der Maasweg 9, Delft 2629HZ, the Netherlands
[b] Proteomics Center, Erasmus University Medical Center, Wytemaweg 80, Rotterdam 3015 CN, the Netherlands
[c] Department of Clinical Genetics and Erasmus MC Center of Expertise for Neurodevelopmental Disorders (ENCORE), Erasmus Medical Center, Rotterdam 3015 GD, the Netherlands
[d] Department of Neuroscience, Erasmus Medical Center, Rotterdam 3015 GD, the Netherlands

ARTICLE INFO

Keywords:
Synaptic cell adhesion
Synapse biology
Animal refinement
Neuronal surface
Proteome
Pull-down proteomics

ABSTRACT

Background: Cell adhesion molecules (CAMs) are membrane-bound proteins that mediate cell-cell interactions through trans-cellular protein complexes. In the context of the neuronal synapse, studies of CAMs have revealed their roles from neuronal recognition and neuronal wiring to synaptic plasticity. CAMs form macromolecular complexes via cis- and trans-interactions; however, identifying the specific proteins in these assemblies is challenging. Their interactions are dynamic and transient, making them difficult to capture, and their hydrophobic transmembrane domains complicate extraction from biological samples.
New method: Here, we present a protocol to pulldown interacting partners of a Teneurin-3-GFP bait protein, as a representative CAM, from minimal mouse brain lysate.
Comparison with existing methods: Affinity purification of a bait protein from a biological sample, followed by mass spectrometry to identify captured prey proteins is a widely used, unbiased approach, though it usually requires large amounts of material. We show that our refined approach detects known Teneurin interactants while substantially reducing the animal tissue required. We further compared detergents used for lysate preparation and found that the total of CAM species enriched in Teneurin-3 samples relative to control varied considerably. Finally, we evaluated different normalization workflows to aid dataset interpretation.
Conclusion: This protocol provides an accessible approach for studying CAM interactions with limited animal tissue, enabling refined insights into the complex protein networks underlying synaptic connectivity.

1. Introduction

In exploring the molecular landscape of neural recognition and adhesion, the study of protein-protein interactions between cell adhesion molecules (CAMs) is essential. CAMs mediate cell-cell adhesion and participate in homophilic binding (to the same molecule) and heterophilic binding (to a different molecule). These interactions can occur at the same cell membrane, also called *cis* interactions, or across opposing cell membranes, referred to as *trans* interactions. This dual binding mode enables CAMs to form large protein assemblies, facilitating the regulation of processes such as transmembrane signaling and the organization of synapses into nanodomains. Importantly, disruption of CAM interactions can severely impair neural circuit wiring and has been linked with various neurological disorders, underscoring their biological significance (Gandawijaya et al., 2021; Gorlewicz and Kaczmarek, 2018; Hillen et al., 2018; Missler et al., 2012). Thus, to fully understand neural circuit wiring, investigating the intricate interactome of CAMs is essential.

Establishing the CAMs interactome poses three major challenges: the transient and low-affinity nature of the interactions (Anton Van Der Merwe and Neil Barclay, 1994), their dynamic regulation, and the inherent hydrophobicity of CAM proteins. To overcome the first two challenges, a range of highly sensitive strategies have been developed, such as cross-linking followed by mass spectrometry analysis (Gonzalez-Lozano et al., 2020; Piersimoni et al., 2022; Matzinger and Mechtler, 2021; Poulopoulos et al., 2012), proximity-labelling followed

* Corresponding author.
E-mail address: d.h.m.meijer@tudelft.nl (D.H. Meijer).

https://doi.org/10.1016/j.jneumeth.2026.110725
Received 12 December 2025; Received in revised form 30 January 2026; Accepted 21 February 2026
Available online 23 February 2026

by mass spectrometry (Roux et al., 2012; Chastney et al., 2020; Dong et al., 2016; Guo et al., 2014; The Integrin Interactome, 2021; Van Itallie et al., 2013; Loh et al., 2016), two-hybrid screening (Causier, 2004; Benincore-Flórez et al., 2022; Li et al., 2011) or ELISA-based screening (Wojtowicz et al., 2020; Ranaivoson et al., 2019; Bushell et al., 2008; Visser et al., 2015). While the above strategies offer important advantages, affinity purification coupled with shotgun proteomic analyses remains the benchmark strategy for resolving CAM complexes (Guo et al., 2014; Savas et al., 2014; Silva et al., 2011; Boucard et al., 2014; Cain et al., 2009; Mohammed and Carroll, 2013; Mayhew et al., 2006; Parcerisas et al., 2021; Elegheert et al., 2017; Ducrot et al., 2025). A common variant of this approach involves pulling down proteins from brain lysates using the extracellular domain of the CAM of interest as bait. However, existing protocols for this method typically require several rodent brains per experiment (Savas et al., 2014; Elegheert et al., 2017; Roy, 2015; Orwick-Rydmark et al., 2016; Rice et al., 2019; Blockus et al., 2021; Savas et al., 2015; González-Calvo et al., 2021). Here, we present a refined protocol for the protein pulldown assay to identify the interactome of a candidate CAM, namely mouse Teneurin-3, using scant mouse brain tissue. Our approach offers significant refinement and reduction in animal use compared to the protocols outlined above, requiring only one-twentieth of a mouse brain per run. Additionally, this protocol overcomes material limitations imposed by small brain size, enabling the study of CAM interactomes in animal models such as *Drosophila* or zebrafish. As mentioned above, the third challenge in studying the interactome of cell adhesion molecules is that many of their interactants are transmembrane proteins, which are challenging to isolate from the cell lysate due to their hydrophobic regions embedded in the lipid bilayer. To extract these proteins, detergents are commonly included in the lysis buffer. However, most protocols use the same detergents without providing a clear rationale for their selection, despite substantial evidence that the type of detergent can significantly affect the recovery of specific membrane proteins (Roy, 2015; Orwick-Rydmark et al., 2016). To address this gap, we tested three different detergents: NP40 IGEPAL, TX-100 frequently used in similar type of assays) and DDM (popular for transmembrane protein solubilization) to assess whether detergent choice influences the diversity of recovered transmembrane proteins. Besides comparing different detergents, we also compared the effect of using different strategies for data normalization on the identification of CAM interactants. We compared no normalization versus mean normalization followed by linear regression, based on the workflow proposed by Aguilan et al. (2020), and quantile normalization, as an alternative method described by Välikangas et al. (2016).

To explore the biological application of this protocol, we focused on Teneurins, a family of CAMs, found at the neuronal synapse, where it plays a role in neuronal recognition and the formation of several brain circuits, notably in the hippocampus and the visual system (Berns et al., 2018; Antinucci et al., 2013; Hunyara et al., 2023; Cheung et al., 2019; Young and Leamey, 2009; Tran et al., 2015). Although the role of Teneurins and the molecular mechanisms by which they participate in the formation of protein complexes are well studied, published efforts to establish its full interactome remain sparse. Proximity labelling of *Drosophila* Ten-m revealed that its intracellular domain interacts with RhoGAP, leading to the activation of Rac1 GTPase, which regulates synaptic partner matching (Xu et al., 2024). Another study aimed to decipher human Teneurin's intracellular interactions using two-hybrid screening, in which it was found that the intracellular domain of TEN-1, when cleaved from the rest of the protein, interacts with HINT1, a transcription inhibitor (Schöler et al., 2015).

These studies have focused on the interactions of Teneurins on the intracellular side, where they play a role in cellular signaling. Regarding the extracellular side of Teneurin, which is involved in synapse recognition and partner matching, numerous publications have identified Teneurins as interactants of Latrophilin. This interaction was first described when establishing the extracellular interactome of Latrophilins (Silva et al., 2011; Boucard et al., 2014; del Toro et al., 2020; Cheung et al., 2022). The molecular mechanism of the Teneurin-Latrophilin complex formation, with a potential third component known as fibronectin leucine-rich transmembrane protein (FLRT), has been investigated using several different structural, biochemical and cellular assays (Boucard et al., 2005; del Toro et al., 2020; Li et al., 2020). To the best of our knowledge, no attempts have been described in the current literature to systematically explore the interactome of Teneurin's extracellular domain. To address this gap, we applied our refined pulldown protocol to study the interactome of one of the Teneurin family members, namely Teneurin-3. Finally, we utilize a cell-clustering assay as a validation strategy to assess whether candidate interactors identified using this protocol are capable of forming trans-cellular interactions with the bait protein. Here, we demonstrate the applicability of this approach by examining interactions between Teneurin-3 and its main interactants identified in our pulldown experiments. Taken together, we present a refined protocol as an accessible strategy for systematically mapping the extracellular interactome of CAMs like Teneurin. This protocol will aid in advancing our understanding of the roles of CAMs in neuronal circuit formation.

2. Results

2.1. Workflow for isolating CAM interactants with limited mouse brain material

To determine the interactome of mouse Teneurin-3 using minimal amount of brain material, we adapted a pulldown protocol for mouse brain (Savas et al., 2014) using GFP-fused Teneurin-3 (Fig. 1A) immobilized on anti-GFP nanobody-coated magnetic beads (Zhang et al., 2019). First, we prepared Teneurin-GFP- or GFP-conditioned media from transfected HEK cells and incubated these with anti-GFP nanobody beads to capture the bait protein (Fig. 1B, step 1–3). In parallel, we prepared brain lysates using three different detergents, NP40, DDM and TX-100 (Fig. 1B, step 4–6). With one adult mouse brain, we were able to generate enough brain lysate to perform triplicate experiments for each detergent condition, for both the Teneurin-3 bait and GFP control proteins. The beads, carrying the Teneurin-3-GFP bait or the GFP control protein, were then incubated with mouse brain lysate to capture potential prey proteins interacting with the bait (Fig. 1B, step 7). To assess the efficiency of our protocol, we performed a Western Blot (WB) analysis (Fig. 1C, D) and SDS-PAGE followed by PAGE-Blue staining (Fig. 1E-G) of samples collected at different steps of the protocol (input, flow-through, brain lysate and pulldown). In the input fractions, we observed a band slightly above 250 kDa in the Teneurin-conditioned media, that is absent in the GFP condition and corresponds to the His-tagged Teneurin bait protein (Fig. 1C, E). This band is also faintly observed in the flowthrough fraction, possibly indicating that the beads were saturated with the bait protein. Each of the three detergent pulldowns displayed a similar intensity for the Teneurin bait protein (Fig. 1D, G), with minimal level of background signal generated by non-specific binding to the brain lysates (Fig. 1F). Of note, the anti-His WB of pulldown material did display background signal, either from partially cleaved Teneurin protein or from non-specific His-protein interactions within the mouse brain lysate (Fig. S1).

2.2. Known CAM interactants identified across all conditions

To assess the effect of different detergents on the cell adhesion molecule interactomes, we performed the pulldown protocol in triplicate for each detergent, namely TX100, NP40, and DDM. The data obtained were then analyzed in three different ways, i.e. 1) without normalization, 2) with a normalization by average followed by linear regression and 3) by quantile normalization (Fig. 2, also see Supplementary Material 1–3). In the mean normalization and linear regression strategy, $\log_2$-transformed iBAQ values were mean-centered and then

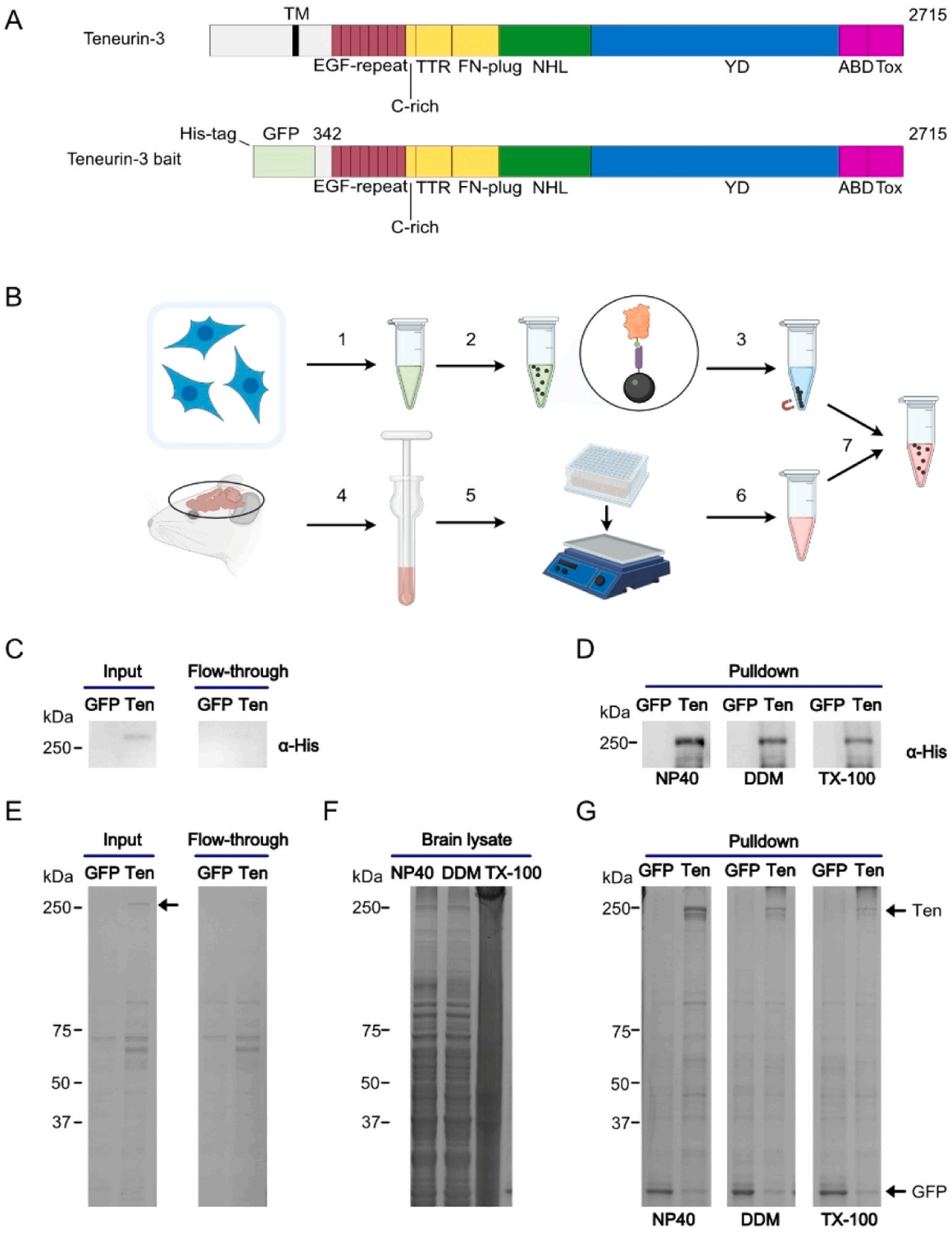

Fig. 1. Workflow pulldown protocol. A - Schematic representation of full-length Teneurin-3 (top) and bait construct used in this study (bottom), consisting of Teneurin-3 fused to a C-terminal His tag and GFP tag. B - Pulldown protocol overview: 1. HEK-E Expression of Teneurin3-ECD fused with an N-terminal GFP tag; 2. Collected cell medium with anti-GFP nanobodies-linked magnetic beads under agitation for 3 h; 3. Magnetic bead pull down; 4. Dissection and homogenization of mouse brain; 5. Adding detergents; 6. The samples were ultracentrifuged and transferred to tubes; 7. The beads linked to the bait protein were transferred to the mouse brain lysate and left for agitation overnight; 8. The beads were pulled down with a magnet and washed from eventual contamination with the lysis buffer. C - Western blot analysis of cell medium samples collected before (input) and after (flowthrough) step 2, comparing the Teneurin-3 bait (Ten) and GFP control. Both constructs include a C-terminal His tag, which was detected using an anti-His antibody. D - Western blot analysis of cell medium samples collected after step 7 with the different detergent conditions (NP40, TX100 and DDM), comparing the Teneurin-3 bait (Ten) and GFP control. E - Coomassie Blue–stained SDS–PAGE gel of cell medium samples collected before and after purification step 2, comparing the Teneurin-3 bait and GFP control. F - The brain lysate samples (NP40, DDM, TX-100) represent lysates prepared using each of the three detergents. G - Coomassie Blue–stained SDS–PAGE gel of cell medium samples collected after step 7 under different detergent conditions (NP40, TX-100, and DDM), comparing the Teneurin-3 bait (Ten) and GFP control.

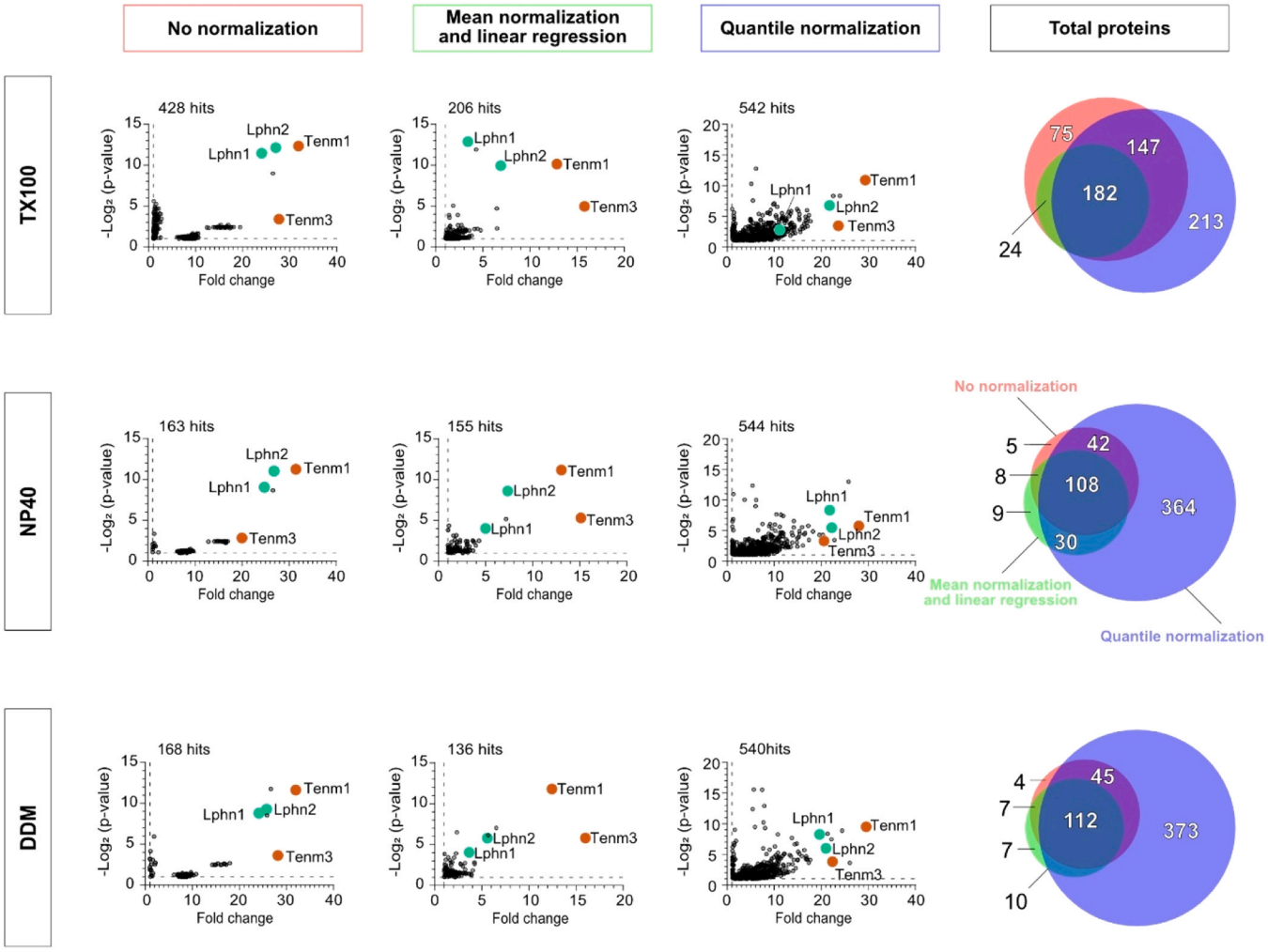

Fig. 2. Volcano Plots generated under three detergent conditions (TX100, NP40, DDM), using three data processing strategies (No normalization, Mean normalization and linear regression, quantile normalization). Dashed lines indicate the applied cut-off of 1 for both fold change and $-\log_2(p)$ value. The number of proteins above that cut-off, referred to as "hits", are indicated at the upper left of each graph. Data points corresponding to Teneurin and Latrophilin family members were highlighted in orange and turquoise, respectively. A Venn diagram at the right illustrates the overlap of hit lists obtained using different normalization strategies.

scaled by the slope of their linear regression against the across-condition average (Fig. S2A, also see supplementary methods). This operation standardizes the dynamic range of values in each sample, making comparisons more straightforward. By reducing technical variability in signal intensity, it ensures that differences between samples more accurately reflect true biological variation rather than experimental artifacts. In the quantile normalization strategy, proteins in each sample are ranked by intensity, and values sharing the same rank across conditions are replaced by their across-condition average (Fig. S2B, also see supplementary methods). Like the first strategy, this approach centers values and standardizes distribution widths, but it imposes stricter normalization by forcing identical distributions across samples through the replacement of individual values with rank-based averages. The steps of data analysis, from raw intensity-based absolute quantification (iBAQ) values to the generation of volcano plots, are detailed in the Supplementary methods, Step-by-step downstream data analysis section.

Teneurins are known to engage in both homophilic interactions (Cheung et al., 2022; Beckmann et al., 2013; Mosca, 2015) and heterophilic interactions, primarily with Latrophilins (Boucard et al., 2014; Burbach and Meijer, 2019; Pederick et al., 2021), which is well reflected in this analysis of the Teneurin-3 interactome. Among the proteins with fold-change values and negative $\log_2$ (p-values) exceeding the selected cut-off of 1, Teneurin-3 (Tenm3), Teneurin-1 (Tenm1), Latrophilin-1 (Lphn1), and Latrophilin-2 (Lphn2) were consistently detected across the different detergent conditions, each with a fold-change greater than 3, independent of the normalization method (Fig. 2). However, normalization had a marked effect on the distribution of data points across conditions. Without normalization, the distribution of the data appears to contain clusters of points with similar fold-change values and p-values (Fig. 2, left panel). Both mean normalizations followed by linear regression and quantile normalization reduce this clustering and lead to a broader dispersion of values, as expected. The relative enrichment of known Teneurin-3 interactants remained largely consistent across different normalization strategies. Note that although Teneurin-3 is artificially introduced as the bait protein, and all intensity values were processed in an unbiased manner, it does not consistently stand out on the volcano plot compared with proteins detected in the pulled down brain material. Nevertheless, the intensity values of Teneurin-3 were 100-fold higher than the rest of the detected proteins, and 257 unique peptides were found for Teneurin-3, indicating its presence as bait protein. Interestingly, the overall number of proteins detected above the cut-off consistently increases when using quantile normalization, compared to mean normalization with linear regression or no normalization at all. In the right panels of the figure, we present a Venn diagram for each detergent condition, illustrating the overlap of proteins detected using these different normalization strategies. The set of proteins identified after quantile normalization encompasses the

majority of those detected with the other two methods.

2.3. Comparison of normalization strategy on CAM interactomes

This overlap raises the question of whether other strategies are filtering out potentially relevant proteins, or if quantile normalization is allowing more background noise into the range of interest. To assess whether the additional proteins identified with quantile normalization cluster into potentially relevant GO terms, we performed functional enrichment analysis on the full hit lists from each normalization strategy using g:Profiler, applying the Benjamini–Hochberg FDR correction with a significance threshold of 0.05 (Kolberg et al., 2023). The GO terms that were significantly enriched relative to the whole dataset as background were not relevant to cell adhesion molecule function, as shown in Fig. S3. Next, we assessed how the normalization strategy affected the detection of functionally relevant proteins, i.e., proteins detected above the defined thresholds (fold-change > 1 and $-\log_2$(p-value) > 1) and associated with the GO categories *cell adhesion* and *cell adhesion molecule binding* (Fig. 3A, Fig. S4). Few proteins in the *cell adhesion* or *cell adhesion molecule binding* categories were found exclusively when the data were unnormalized or normalized using mean and slope correction (Fig. 3A). Conversely, many proteins in these categories were detected above the threshold only when using quantile normalization. Among them, several represent strong candidates for interacting with Teneurin in the context of neuronal cell adhesion, including Contactin-1 (Cntn1), Neural Cell Adhesion Molecule-1 (Ncam1), ADAM Metallopeptidase Domain-22

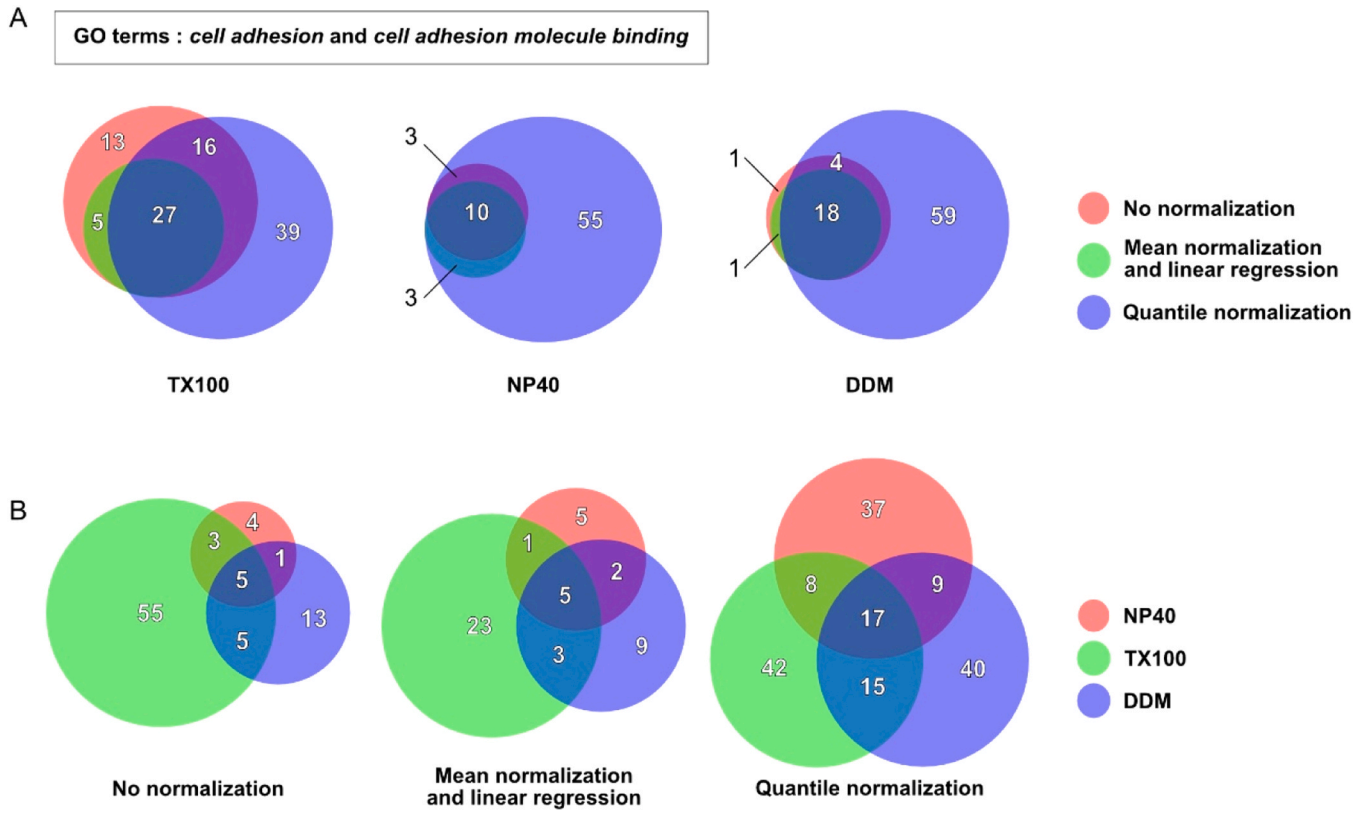

C

TX100		
ALL		
Tenm1	Prdx6	Trim29
Adgrl1	Serbp1	Nptn
Tenm3	Rpl15	Rpl29
Pdlim1	Hdlbp	Parva
Nfasc	Dsg4	Rpl7a
Adam15	Crnn	Hspd1
Tln2	Pdia3	Prdx2
Pdlim5	Csrp1	Tmpo
Rsl1d1	Dsg3	Pkp3

NP40	
ALL	
Tenm1	Lypla2
Adgrl1	Calr
Tenm3	Dsg4
Dchs1	Dsg3
Fgg	Dhps

DDM	
ALL	
Tenm1	Calr
Adgrl1	Eps15
Tenm3	Lrrc59
Rsl1d1	Vamp3
Dchs1	Dsg3
Scyl1	Ly6d
Krt18	Hapln1
Pdlim5	Smarca4
Smarcb1	Smarca2

D

No normalization
ALL
Tenm1
Adgrl1
Tenm3
Dchs1
Dsg3

Mean normalization and linear regression
ALL
Tenm1
Tenm3
Adgrl1
Rsl1d1
Dsg3

Quantile normalization	
ALL	
Adgrl1	Tln1
Tenm1	Hspa5
Tln2	Clasp1
Tenm3	Dsg3
Rsl1d1	Pdia3
Ckap5	Dsg4
Calr	Dlg4
Ptpn11	Glmn
Map4k4	

Fig. 3. Distribution of functionally relevant proteins detected under different normalization strategies and detergent conditions. A - Venn diagrams of top-listed proteins associated with relevant GO terms (cell adhesion and cell adhesion molecule binding) identified in pulldown experiments using three different normalization strategies under TX100, NP40, and DDM detergent conditions. The full protein lists associated with the diagrams are shown in Fig S4B. - Venn diagrams of top-listed proteins associated with relevant GO terms (cell adhesion and cell adhesion molecule binding) identified in pulldown experiments using three different detergent conditions (TX100, NP40, and DDM) under each normalization strategy. C - Proteins associated with relevant GO terms (cell adhesion and cell adhesion molecule binding) consistently detected across all normalization strategies within each detergent condition. D- Proteins associated with relevant GO terms (cell adhesion and cell adhesion molecule binding) consistently detected across all detergent conditions using each normalization strategy.

(Adam22), Reticulon-4 (Rtn4), Catenin Delta-1 (Ctnnd1), Cerebellin-1 precursor (Cbln1), Tenascin R (Tnr), Desmoglein- 4 (Dsg4), and Testican-2 (Spock2) (Fig. S4, Fig. S5). This indicates that while quantile normalization appears less efficient than mean and slope correction at distinguishing known Teneurin interactants from other proteins, many potential candidates could be missed when not applying this normalization method. In the context of interactome profiling, such an outcome is undesirable. Thus, it seems advisable to apply multiple normalization strategies before establishing a final list of potential new interactants.

2.4. Choice of detergent affects identification of novel potential CAM interactants

Next, we compared the performance of each detergent in detecting functionally relevant proteins belonging to the GO terms *cell adhesion* and *cell adhesion molecule binding* with each normalization strategies (Fig. 3A, D). This comparison indicates that in the TX100 condition a larger proportion of proteins were detected above the threshold that are classified as cell adhesion, or cell adhesion molecule binding terms. Notably, the known interacting proteins of Teneurin-3 are consistently detected across all three detergent conditions, regardless of the normalization strategy (Fig. 2, Fig. 3D), namely Teneurin-1, Latrophilin-1 and Latrophilin-2, as well as the bait Teneurin-3. Several novel candidates were also identified across at least two out of three detergent conditions, for instance, Desmoglein-3 and -4 (Dsg3, Dsg4), Dachsous Cadherin-Related-1 (Dchs1), or Glycoprotein M6B (Gpm6b) (Fig. 3D, Fig. S6). Importantly, some of the proteins uniquely detected in a single detergent condition represent promising candidates for potential interaction with Teneurin, based on their nature, function, or subcellular localization, for instance, Neurofascin (Nfsc), Tenascin R (Tnr), Contactin-1 (Cntn1) and Reticulon-4 (Rtn4) (Fig. S6). These data indicate that the use of different detergents has a significant effect on identification of potentially relevant proteins. Thus, testing different detergent conditions when establishing a protein's membrane interactome is important to capture a more complete hit-list.

2.5. Choice of detergent affects peptide coverage of known interactions

Beyond the detection of distinct CAMs across detergent conditions, an additional parameter to consider is the recovery of known interactants. As shown in Fig. 2, Latrophilin-1, Latrophilin-2, and Teneurin-1 were enriched in all detergent conditions, confirming the robustness of their association with the bait. However, their peptide coverage revealed detergent-dependent differences, indicating variations in recovery efficiency (Fig. 3, Supplementary material 4). We did not consider Teneurin-3 in this analysis, as its extracellular domain constituted the bait protein, and its coverage does not reflect the ability of each detergent to isolate it from the membrane. Additionally, no peptides mapping to the intracellular or transmembrane domains of Teneurin-3 were detected, arguing against significant co-purification of endogenous Teneurin-3 from the brain lysate (Supplementary material 5). Interestingly, Teneurin-1 was identified by only one or two unique peptides in the NP40 and TX100 conditions respectively and not identified at all using DDM (Fig. 4A, B). Its prominent presence in the volcano plots of the TX100 and NP40 condition, and in addition its presence in the DDM condition however may be due to shared peptides with the bait protein (59,22 % identity between mouse Teneurin-3 and Teneurin-1). Using NP40 as detergent results in a substantial increase in the number of identified peptides for Latrophilin-1, compared to TX100 and DDM (Fig. 4C). This is also the case for Latrophilin-2, albeit at a lesser extent (Fig. 4D).

A

Teneurin-1						
peptide	NP40		TX100		DDM	
	Ten	GFP	Ten	GFP	Ten	GFP
APSSLAVSPDGTLYVADLGNVR	8,43		8,93			
SVMLLLHSQR			8,33			
Coverage (%)	0,81%		1,17%		0%	

B

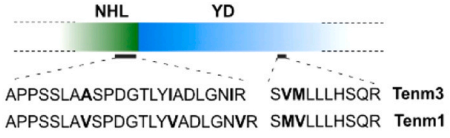

C

Latrophilin-1						
peptide	NP40		TX100		DDM	
	Ten	GFP	Ten	GFP	Ten	GFP
AVVETVDNLLRPEALESWK	14,83					
CPGSDVIMVENANYGR	7,71				7,912	
DNQLYVWNNYFVVR	7,06					
ELACEGYPIELR	7,82				7,58	
GIASFQCLPALGLWNPR	7,81		7,30			
GSIYAGDVSSSVK	16,25		7,742		15,92	
IKSGETVINTANYHDTSPYR	7,64				7,264	
IYVMPWIPYR	7,00					
LAGEAGTGGPGGASLVVNSQVIAASINK	7,38					
LAGEAGTGGPGGASLVVNSQVIAASINKESSR	15,95					
LVVSQLNPYTLR	23,95		8,274		15,85	
RVQWPATQQGMLVERPCPK	15,25				7,936	
SASNAFMVCGVLYVLR	7,78				7,525	
SGENAANIASELAR	8,33		8,108		8,383	
SMLGYWSTQGCR	7,76					
VFLMDPVIFTVAHLEAK	8,32		8,28		8,27	
VFVCPGTLQK	7,84					
VLEPTSTHESEHQSGAWCK	7,56					
Coverage (%)	20,40%		6,34%		6,68%	

D

Latrophilin-2						
peptide	NP40		TX100		DDM	
	Ten	GFP	Ten	GFP	Ten	GFP
AALPFGLVR	15,08				7,42	
AASNAFMICGVLYVVR	15,98		15,74		15,46	
AIVDSPCIYEAEQK	24,81		25,12		16,53	
AIVDTVDNLLR	16,46		16,55		7,79	
CPGSDVIMIESANYGR	7,78		7,56			
DNQLYVWNNNFILR	23,08		23,96		22,95	
ELSCEGYSIDLR	24,05				8,34	
GEYVDVPFPNQYQYIAAVDYNPR	7,44				7,59	
GMMVERPCPK	16,47		16,11		16,10	
LMEQLVDILDAQLQELKPSEK	8,79				8,58	
LMEQLVDILDAQLQELKPSEKDSAGR	7,56		7,50			
SGEAIINYANYHDTSPYR	7,91		16,42		16,27	
SGENAASLANELAK	8,59		8,69		8,56	
TDDKICDADPFQMENTDCYLPDAFK	7,85		7,61		7,58	
TQCIVVTGSDVFPDPCPGTYK	8,09				7,84	
VFVCPGTLK	8,75					
YLEVQYECVPYMEQK	24,26		24,23		23,41	
Coverage (%)	18,87%		15,22%		15,43%	

Fig. 4. Peptide coverage of known Teneurin-3 interactants detected in the pulldown assay. The coverage is indicated in percentage for each condition at the bottom of each tab. A - Detected peptides and corresponding MS intensities for Teneurin-1 under different detergent conditions. B - Sequences and positions of the detected Teneurin-1 peptides, aligned with the corresponding regions of Teneurin-3. C - Detected peptides and corresponding MS intensities for Latrophilin-1 under different detergent conditions. D - Detected peptides and corresponding MS intensities for Latrophilin-2 under different detergent conditions.

2.6. Cell clustering assay as a validation strategy for Teneurin-3 trans-interactors

The mass spectrometry analysis described above yielded a list of CAMs that were enriched in the Teneurin-3 bait condition compared to the GFP control, suggesting that they may represent potential interactors of Teneurin-3. However, the existence of such interactions still requires experimental validation. To this end, we propose a quantitative cell-clustering assay to assess protein *trans*-cellular interactions. In this assay, plasmids encoding either full-length or membrane-tethered bait proteins fused to a fluorescent tag, as well as candidate interactors fused to a distinct fluorescent tag, are electroporated into K562 cells. K562 cells are a non-adherent leukemia cell line that does not express endogenous cell adhesion molecules and therefore does not spontaneously form clusters. Following electroporation, cells expressing the different proteins are mixed and transferred to cluster-formation medium. Here, we demonstrate this assay using Teneurin-3 and interactors identified in our pulldown data, namely Latrophilin-2, Teneurin-1, and Teneurin-3 itself. We performed this assay while taking into account the alternative splicing of two micro-exons of Teneurin-3, termed A and B (Berns et al., 2018; Gogou et al., 2024) (Fig. 5A). We assayed all splice variants of Teneurin-3, namely A0B0, A0B1, A1B0, and A1B1, where "1" indicates the presence and "0" the absence of splice inserts A or B. Interestingly, heterotypic interactions between Teneurin-3 and Latrophilin-2 displayed an opposite splice-variant dependence compared to the homotypic interactions involving Teneurin-3 and Teneurin-1. Specifically, Latrophilin-2 formed clusters with all Teneurin-3 splice variants except A0B1 (Fig. 5B–C). In contrast, Teneurin-1 showed clustering exclusively with the Teneurin-3 A0B1 splice variant (Fig. 5D, E). Finally, Teneurin-3 A0B1 formed clusters with all other Teneurin-3 splice variants (Fig. 5F, G). Previous data have already indicated that in terms of homophilic clustering of all splice variants, A0B1 has the highest propensity of clustering (Gogou et al., 2024). At first glance, the splice-dependent nature of Teneurin-3 homotypic interactions might raise questions regarding the detection of Teneurin-1 and Teneurin-3 in our pulldown experiments, as the bait protein used was the Teneurin-3 A0B0 variant. However, previous studies on Teneurin-2 have shown that the effect of the B splice insert on interaction specificity is observed only in a membrane-bound context and not when one of the interaction partners is in solution, as is the case in our pulldown experiments (Li et al., 2020; Araç and Li, 2019; Li et al., 2018). Moreover, none of the Teneurin-3 peptides detected in our pulldown data contained the A or B splice inserts. Additionally, peptides that confirmed the absence of splice insert A and splice insert B, by covering the exon boundaries, were identified (Supplemental Material 5). Taken together, in addition to using cell clustering assays as validation strategy for our refined pulldown protocol, these results indicate that the splice-dependent modulation of Teneurin-Latrophilin interactions previously described for Teneurin-2 is also observed for Teneurin-3.

3. Discussion

The workflow and datasets presented here demonstrate a refined pulldown protocol to establish the Teneurin interactome from minimal amount of mouse brain tissue. We achieved a substantial reduction in input material, performing effective pulldowns using only one-twentieth of a mouse brain per run, compared to at least one rodent brain used in previous published methods (Savas et al., 2014; Elegheert et al., 2017; Rice et al., 2019; Savas et al., 2015; González-Calvo et al., 2021). This was made possible by two key improvements to the protocol: first, the direct coupling of bait proteins to magnetic beads, which eliminated the need for a separate bait pulldown step and likely enhanced bait protein stability and quality; and second, the sensitivity of current mass spectrometry platforms, which enables confident detection of interactants despite the lower input. Importantly, this reduction in material promotes refinement and reduction in animal use, contributing to more ethical and efficient experimental designs. These advances significantly increase the scalability of our approach, for instance towards including more detergents for comparison. However, any further reductions in input material may be limited by the sensitivity thresholds of mass spectrometry, beyond which specific interactants may fall below the level of detection.

In our effort to obtain increased insights into the function of CAMs in synapse formation, we identified the interacting proteins of Teneurin-3. Known interactants Latrophilin-1, Latrophilin-2, and Teneurin-1 were confidently confirmed with our refined pulldown protocol. No unique peptides were detected for Teneurin-2, Teneurin-4, or Latrophilin-3 proteins. It remains possible that these proteins were indeed pulled down by the Teneurin- 3 bait but excluded from the analysis due to shared peptides with other Teneurin (Teneurin-3 shares 66.4 % sequence identity with Teneurin-4 and 67.9 % with Teneurin-2 in mouse) or Latrophilin family members (Latrophilin-3 shares 59.8 % with Latrophilin-1 and 59,2 % with Latrohphilin-2 in mouse). Latrophilins are known to form a multiprotein complex with Teneurin and members of the fibronectin leucine rich transmembrane protein (FLRT) family (del Toro et al., 2020; Burbach and Meijer, 2019; Sando et al., 2019). In the publication of Savas et al. (2014) (Savas et al., 2014), a similar pulldown strategy using Latrophilin as bait resulted in the detection of both FLRT and Teneurin. The absence of FLRT in our dataset may be explained by the fact that Teneurin is part of this complex through its interaction with Latrophilin and does not directly bind to FLRT.

In addition to these known interactants, we observed enrichment of other synaptic cell-adhesion proteins in the Teneurin-bait condition compared to the GFP control. However, the composition of this enriched set varied depending on the normalization strategy and the detergent condition. To confirm these potential interactions, additional experiments are required, such as the proposed cell-clustering assay or, alternatively, techniques including surface plasmon resonance, cross-linking, or proximity ligation assays.

To choose a normalization strategy for our dataset, we turned to the work of Välikangas et al. (2016), who recommended applying normalization and found only modest differences between methods. Their evaluation focused on three criteria: reduction of technical variation, accurate detection of truly differentially expressed proteins, and agreement between observed and theoretical fold-changes. In our study, we compared quantile normalization, one of the methods assessed by Valikangas et al., to normalization by averaging followed by slope correction, as recommended by Aguilan et al. (2020) as well as to unnormalized data. Specifically, we assessed how each method affected the consistency of fold change values for Teneurin-3 and known interactants of Teneurin-3 and the number of potentially relevant proteins detected above the selected cut-off. We found that data treatment by mean normalization and linear regression yielded more consistent fold changes for these known interactants than either quantile normalization or unnormalized data. This approach also improved the appearance of data distribution. Notably, quantile normalization resulted in a substantial increase in the number of proteins identified above the cut-off, including several of biological relevance. This effect is likely driven by the way quantile normalization ignores the original values and replaces them according to rank, forcing all samples to share the same distribution. Since this process alters the relative distances between proteins, it can generate larger numerical differences between conditions and thereby inflate fold-change values. Based on these findings, we recommend comparing multiple normalization strategies before defining the final list of candidate interactants for downstream validation.

Regarding detergent optimization, this is rarely addressed in shotgun proteomics workflows. To assess whether different detergents preferentially solubilize specific transmembrane proteins, an ANOVA test was performed on samples pulled down with Teneurin-3 across the various detergent conditions. Of the 2479 proteins detected, 49 showed

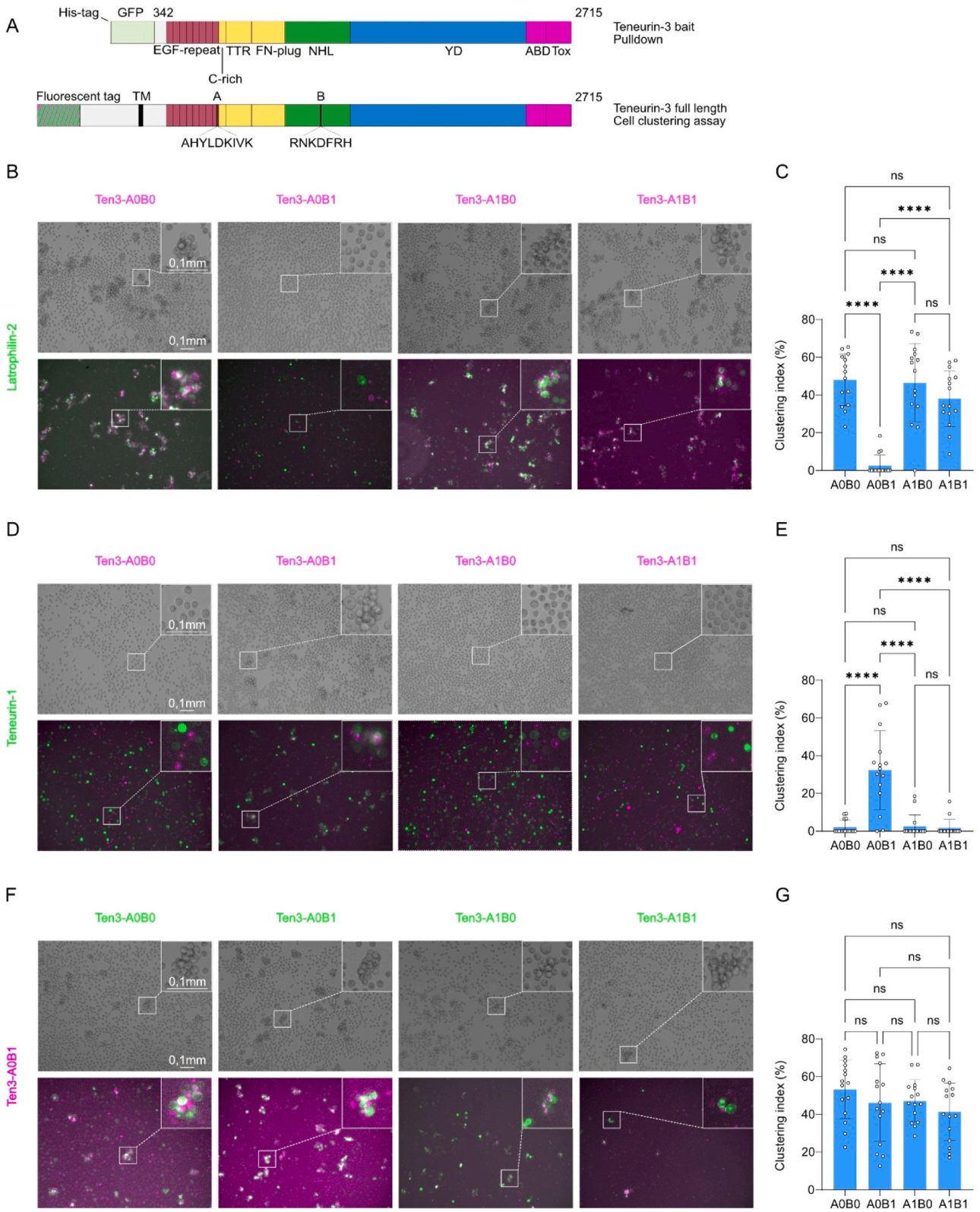

Fig. 5. Validation of trans-interactions between Teneurin-3 and known interacting partners using clustering assay. A - Schematic of Teneurin-3 A0B0 used as bait protein in the pulldown experiment and Teneurin-3 Full length with a fluorescent tag and alternatively spliced insert as used in the clustering assay. B - Representative greyscale and fluorescence images showing the four Teneurin-3 splice variants (A0B0, A0B1, A1B0, and A1B1; magenta) co-expressed with Latrophilin-2 (green), including a 3 × magnified inset. C - The clustering index was calculated as the ratio of the total surface area of all clusters to the total surface area of all identified regions of interest (ROIs). Statistical significance was assessed using a one-way ANOVA. Quantification was performed on five images per condition across three technical replicates, yielding a total of 15 data points per condition. D - Representative greyscale and fluorescence images showing the four Teneurin-3 splice variants (magenta) co-expressed with Teneurin-1 (green). E - Clustering index between Teneurin-3 splice variants and Teneurin-1. F - Representative greyscale and fluorescence images showing the four Teneurin-3 splice variants (green) and Teneurin-3 A0B1 (magenta). G - Clustering index between Teneurin-3 splice variants and Teneurin-3 A0B1.

statistically significant differences between conditions (ANOVA $p < 0.05$), but only 6 of these were transmembrane proteins (Fig. S7, Supplementary material 4). Moreover, the choice of detergent did not influence the detection of known Teneurin-3 interactants above the selected cut-off. However, detergent composition had a marked impact on the detection of other potentially relevant proteins. Based on these findings, we recommend optimizing the detergent composition of the lysis buffer when preparing biological samples for membrane interactome studies. In the context of Teneurin interactome analysis, 1 % NP40 proved optimal, providing the most comprehensive protein coverage for Teneurin-1, Latrophilin-1, and Latrophilin-2 (Fig. 4). However, the use of TX100 resulted in the detection of a higher number of proteins within GO categories relevant to screening for CAM interactomes (Fig. 3). Therefore, to identify potential new interactants of Teneurin-3, we recommend using TX100.

In addition to providing a refined protocol for establishing the interactome of cell adhesion molecules at the neuronal synapse, we address a CAM interactions knowledge gap by presenting a list of potential interactants of Teneurin-3. We believe that the data generated and the use of our method in future research will contribute to the understanding of the molecular basis of neuronal circuit formation.

4. Methods

4.1. Mouse brain tissue

Mouse left-over brain tissue was provided by the lab of Geeske van Woerden, (Erasmus MC) and derived from pregnant mice whose litters were used for the preparation of primary neuronal cultures for unrelated research projects. All experiments with animals were conducted in accordance with the European Commission Council Directive 2010/63/EU (CCD project license AVD101002017893), and all described experiments and protocols were ethically approved by an independent review board of the Erasmus MC

4.2. Vectors and cloning

The plasmid encoding the N-terminally GFP-tagged full ECD of mouse Teneurin-3 (residues 312–2715, excluding splice insert A or B) was created by subcloning the full ECD (Biocat) into the pUPE106.03 GFP vector containing a N-terminal cystatin secretion signal and N-terminal His6 tag (U-Protein Express) using *Bam*H1 and *Not*I cloning sites. Full-length mouse Lphn2 (clone BC172691, Biocat GmbH) was amplified by PCR and cloned into the pmEGFP-N1 backbone (catalog number 54767, Addgene), containing a C-terminal GFP tag by using the *Nhe*I and *Bam*HI restriction sites. Full-length mouse Teneurin-1 (Biocat, catalog number BC138861, name pCR-XL-mODZ1) was amplified by PCR and cloned into the pmEGFP-N1 backbone (catalog number 54767, Addgene), containing a C-terminal GFP tag by using the *Bam*HI and *Not*I restriction sites added to the PCR primers. Full-length mouse Teneurin-3 A0B0 was subcloned from the previously described GFP-tagged construct into the mCherry2-C1 backbone (catalog number 54563, Addgene) using the restriction sites *Bam*HI and *Not*I. The mCherry2-C1 backbone was previously made compatible to *Bam*HI/*Not*I cloning using primers designed to delete the multiple cloning site and to add the *Bam*HI/*Not*I restriction sites. Full-length mCherry-tagged splice variants Ten3-A0B1, Ten3-A1B0 and Ten3-A1B1 previously described in Gogou et al. (2024) were cloned into full-length mCherry-Ten3-A0B0 using the restriction sites *Hin*dIII and *Not*I.

4.3. Cell culture

Epstein–Barr virus nuclear antigen I-expressing HEK293 cells (HEK-E; U-Protein Express) were cultured in FreeStyle293 expression medium with GlutaMAX (FreeStyle; Gibco) supplemented with 0.2 % fetal bovine serum (FBS, Gibco) and 0.1 % Geneticin (G418 Sulfate; Gibco). Cells were grown at 37°C and 5 % CO2.

4.4. Transfection

$0{,}32*10^6$cells/mL were plated in 5 mL of FreeStyle293 expression medium with GlutaMAX (FreeStyle; Gibco). After 24 h, 7.5 ug of PEI were mixed with 2.5 ug of DNA in 200uL of OPTIMEM per condition. After 20 min incubation at room temperature, this mix was added on the cells. 500uL of medium supplemented with 5,5 % Primatone was added to the cells 6 h after transfection. The cell medium was harvested 6 days after transfection, after centrifugating the cells at 300 g for 10 min. The medium containing the bait protein was then kept at −20°C.

4.5. Affinity pulldown

Mouse brain was homogenized in 150 mM NaCl 20 mM HEPES buffer (3,6 mL/brain) using a glass Dounce homogenizer. Sonication was performed 3x 10 sec with a 30 sec pause between each pulse with an amplitude of 40 %. CaCl2 and MgCL2 were added to the concentration of 2 mM, Complete Protease inhibitor (Roche) and 1 % detergent (TX-100, DDM or NP-40 IGEPAL). The lysates were then incubated at 4°C O/N with a gentle agitation, preventing bubbles to form. The next day the lysates were diluted to a final volume of 3 mL and centrifuged at 72300RPM for 1 h at 4°C, which concentration in protein ranged between 1,2 and 1,5 mg/mL. The anti-GFP magnetic beads (Chromotek) were washed 3 times with 0.5 mL of PBS using Eppendorf magnetic rack. Then 1 mL of HEK-E cell medium containing the GFP fusion bait protein was put on the beads at rotation for 2h30 at 4°C. The beads were washed three times with detergent-free lysis buffer (150 mM NaCl, 20 mM HEPES, complete protease inhibitor, 2 mM CaCl2 and 2 mM MgCl2). 300 µL of lysis buffer was then put on the beads and incubated on rotation O/N at 4°C. After removing the supernatant, the beads were washed 3 times with the corresponding lysis buffer (150 mM NaCl, 20 mM HEPES, complete protease inhibitor, 2 mM CaCl2, 2 mM MgCl2, 1 % detergent)

4.6. SDS-PAGE and western blot

Samples were diluted 1.5-fold in sample buffer (30 % w/v glycerol, 6 % SDS, 0.03 % bromophenol blue, 187.5 mM Tris, 0.06 % β-mercaptoethanol) and boiled at 98°C for 10 min. SurePAGE™, Bis-Tris, 10 × 8, 4–12 %, 15-well gels (GenScript) were loaded with 14 µL of the heated sample and electrophoresed at 200 V for 30 min. Gels were either stained using InstantBlue Coomassie Protein Stain (Abcam) and imaged with a Chemidoc imager (Bio-Rad), or transferred to a membrane using the Trans-Blot Turbo Transfer System (Bio-Rad) for western blotting.

The membrane was blocked in 15 mL of 3 % BSA (Carl Roth) prepared in TBS-T buffer (20 mM Tris, 150 mM NaCl, 0.1 % Tween 20) for 1 h at room temperature. It was then incubated overnight at 4°C with primary antibodies (0.5 µL anti-6xHis tag, Thermo Fisher, diluted in 1 mL TBS-T buffer). Following three 10 min washes in 10–15 mL TBS-T buffer, the membrane was incubated with secondary antibodies (2 µL HRP-conjugated anti-mouse diluted in 10 mL TBS-T buffer) for ~h at room temperature. After another three 10-min washes in 10–15 mL TBS-T buffer, chemiluminescent detection was performed using a two-component luminol enhancer solution (Thermo Scientific) for 5 min, and the signal was captured with a Chemidoc imager (Bio-Rad).

4.7. Mass spectrometry data acquisition

For IP-MS, proteins were digested on-bead with sequencing grade trypsin (1:100 (w:w), Roche) overnight at room temperature. Protein digests were desalted using a C18 Stagetip (2 plugs of 3 M Empore C18) and eluted with 80 % acetonitrile and dried in a Speedvac centrifuge. Peptides were then analyzed by nanoflow LC-MS/MS as described below.

Nanoflow LC-MS/MS was performed on an EASY-nLC system (Thermo) coupled to an Orbitrap Lumos mass spectrometer (both ThermoFisher Scientific) or on a Vanquish Neo LC system (Thermo) coupled to an Orbitrap Exploris 480 (Thermo), all operating in positive mode and equipped with a nanospray source. Peptide mixtures were trapped on a PepMap trapping column (2 cm × 100 μm, Thermo, 164750) at a flow rate of 1 μl/min. Peptide separation was performed on ReproSil C18 reversed phase column (Dr Maisch GmbH; column dimensions 25 cm × 75 μm, packed in-house) using a linear gradient from 0 % to 80 % B (A = 0.1 % FA; B = 80 % (v/v) AcN, 0.1 % FA) in 120 min and at a constant flow rate of 250 nl/min. The column eluent was directly sprayed into the ESI source of the mass spectrometer.

All mass spectra were acquired in profile mode and the resolution in MS1 mode was set to 120,000 (automatic gain control (AGC) target: 4E5) and the *m/z* range to 350–1400. Fragmentation of precursors was performed in 2 s cycle time data-dependent mode by higher-energy collisional dissociation (HCD, or beam-type collision induced dissociation (CID)) with a precursor window of 1.6 *m/z* and a normalized collision energy of 30.0; MS2 spectra were recorded in the orbitrap at 30,000 resolution. Singly charged precursors were excluded from fragmentation and the dynamic exclusion was set to 60 s.

4.8. Data analysis

DDA raw data files were analyzed using the MaxQuant software suite (version 2.2.0.0, www.maxquant.org[64](Tyanova et al., 2016) for the identification and relative quantification of proteins. 'Match between runs' was disabled and a false discovery rate (FDR) of 0.01 for peptides and proteins and a minimum peptide length of 6 amino acids were required. The Andromeda search engine was used to search the MS/MS spectra against the *Mus musculus* Uniprot database (version May 2022) concatenated with the reversed versions of all sequences and a contaminant database listing typical background proteins. A maximum of two missed cleavages were allowed. MS/MS spectra were analyzed using MaxQuant's default settings for Orbitrap and ion trap spectra. The maximum precursor ion charge state used for searching was 7 and the enzyme specificity was set to trypsin. Further modifications were cysteine carbamidomethylation (fixed) as well as methionine oxidation (variable). The minimum number of peptides for positive protein identification was set to 2. The minimum number of razor and unique peptides set to 1. Only unique and razor non-modified, methionine oxidized and protein N-terminal acetylated peptides were used for protein quantitation. The minimal score for modified peptides was set to 40 (default value).

4.9. Downstream data analysis

The data were normalized either using mean normalization, followed by linear regression or quantile normalization. Alternatively, the data were not normalized and only $\log_2$ transformed. After normalization, volcano plot were generated by calculating the fold change as the difference in protein abundances, derived from intensity-based absolute quantification (iBAQ) values, between the Teneurin-GFP bait condition and the GFP control, followed by a parametric paired one-tailed *t*-test. Fold-change values between the Teneurin-3 bait and GFP control conditions, along with $\log_2$(p-values) obtained from a *t*-test, were both subjected to a cut-off of 1. For the fold- change, this cut-off selects proteins that are more abundant in the bait condition compared to the GFP control. For the -$\log_2$(p-value), it corresponds to a p-value below 0.5. This threshold was intentionally chosen to be lenient, as more stringent criteria may exclude potentially relevant interaction candidates. In proteomic shotgun assays of this type, variability between replicates and low peptide coverage can lead to underestimation of biologically meaningful interactions, particularly for low-abundance or transient binding partners. The steps of data analysis, from raw mass spectrometry intensities to the generation of these volcano plots, are detailed in the supplemental methods section titled Mass Spectrometry Data Analysis.

4.10. Cell clustering assay

K562 cells (Leibniz Institute DSMZ, ACC 10) were maintained in RPMI-1640 medium (Gibco) supplemented with 10 % fetal bovine serum and 1 % penicillin–streptomycin (Gibco) and cultured in suspension at 37 °C with 5 % CO_2 under shaking conditions. For electroporation, cells were collected by centrifugation at 300 g for 5 min, washed once in 1 × PBS (Gibco), centrifuged again, and resuspended in buffer R (Gibco). A total of 2×10^6 cells were prepared per condition and incubated with 15 μg of plasmid DNA (maintaining a gene-containing vector to empty vector ratio of 1:5) for 15 min at room temperature. Electroporation was performed using the Neon Transfection System (Thermo Fisher Scientific) with settings of 1450 V, a 10 ms pulse duration, and three pulses (Pederick et al., 2021; Chataigner et al., 2022). Immediately after transfection, cells were transferred into six-well plates containing 5 mL of pre-warmed RPMI-1640 medium supplemented with 10 % FBS and incubated for approximately 20 h under the same shaking culture conditions. Cells were then imaged using an EVOS M5000 microscope (Thermo Fisher Scientific) equipped with a 10 × objective (NA = 0.25) and a GFP LED light cube. Imaging was performed in a blinded manner to eliminate potential bias in the assessment of clustering behavior.

GFP and RFP channel images were merged and processed in Fiji, following background subtraction using the rolling-ball algorithm with a 50-pixel radius. Regions of interest (ROIs) exceeding 100 pixels were detected using the Analyze Particles function and measured. Clusters were defined as ROIs with an area of at least 2000 pixels (corresponding to approximately four adjacent cells). The clustering index was calculated as the total area of all clusters divided by the total area of all ROIs (clustered and non-clustered), multiplied by 100 %. Both cluster size and clustering index were averaged per image. For each condition, 15 images across three independent experiments (five images per experiment) were analyzed. Statistical comparisons were performed using one-way ANOVA followed by Tukey's multiple-comparisons test in GraphPad Prism (GraphPad Software, San Diego, CA). Results are presented as mean ± SEM.

Authorship statement

Agathe Henocq performed the experiments, conducted data analysis, prepared figures, and wrote the original draft. Wouter Doff, Dick Dekkers and Jeroen A. A. Demmers carried out the mass spectrometry measurements and contributed to data interpretation. Geeske van Woerden coordinated animal care and housing, and provided the mouse brain material essential to this study. Dimphna H. Meijer supervised the project and edited the manuscript. All authors reviewed and approved the final manuscript.

CRediT authorship contribution statement

Dimphna H. Meijer: Writing – review & editing, Supervision, Funding acquisition, Data curation, Conceptualization. **Geeske M. van Woerden:** Writing – review & editing, Resources. **Demmers Jeroen A. A.:** Writing – review & editing, Software, Resources, Methodology, Formal analysis. **Wouter Doff:** Software, Methodology, Formal analysis, Data curation. **Dick Dekkers:** Software, Methodology, Formal analysis, Data curation. **Henocq Agathe Marie:** Writing – review & editing, Writing – original draft, Visualization, Methodology, Investigation, Data curation, Conceptualization.

Declaration of generative AI and AI-assisted technologies in the manuscript preparation process

During the preparation of this work the author used ChatGPT in order to correct English grammar mistakes. After using this tool/service, the author reviewed and edited the content as needed and takes full responsibility for the content of the published article.

Declaration of Competing Interest

The authors declare that they have no known competing financial interests or personal relationships that could have appeared to influence the work reported in this paper.

Acknowledgements

We would like to acknowledge Anouk Heuvelmans and Angelica Casotto for their contribution in collecting mice brain, as well as Christos Gogou and Koen Wentinck for their help in optimizing the brain lysates preparation

Appendix A. Supporting information

Supplementary data associated with this article can be found in the online version at doi:10.1016/j.jneumeth.2026.110725.

Data availability

The raw mass spectrometry data are available on PRIDE : http://www.ebi.ac.uk/pride Project accession: PXD071541 Token: igbzyHG7GM0v

References

Aguilan, J.T., Kulej, K., Sidoli, S., 2020. Guide for protein fold change and *p* -value calculation for non-experts in proteomics. Mol. Omics 16, 573–582.
Antinucci, P., Nikolaou, N., Meyer, M.P., Hindges, R., 2013. Teneurin-3 specifies morphological and functional connectivity of retinal ganglion cells in the vertebrate visual system. Cell Rep. 5, 582–592.
Anton Van Der Merwe, P., Neil Barclay, A., 1994. Transient intercellular adhesion: the importance of weak protein-protein interactions. Trends Biochem. Sci. 19, 354–358.
Araç, D., Li, J., 2019. Teneurin structure: splice variants of a bacterial toxin homolog specifies synaptic connections. Front. Neurosci. 13, 838.
Beckmann, J., Schubert, R., Chiquet-Ehrismann, R., Müller, D.J., 2013. Deciphering teneurin domains that facilitate cellular recognition, cell–cell adhesion, and neurite outgrowth using atomic force microscopy-based single-cell force spectroscopy. Nano Lett. 13, 2937–2946.
Benincore-Flórez, E., et al., 2022. Iduronate-2-sulfatase interactome: validation by yeast two-hybrid assay. Heliyon 8, e09031.
Berns, D.S., DeNardo, L.A., Pederick, D.T., Luo, L., 2018. Teneurin-3 controls topographic circuit assembly in the hippocampus. Nature 554, 328–333.
Blockus, H., et al., 2021. Synaptogenic activity of the axon guidance molecule Robo2 underlies hippocampal circuit function. Cell Rep. 37, 109828.
Boucard, A.A., Chubykin, A.A., Comoletti, D., Taylor, P., Südhof, T.C., 2005. A splice code for trans-synaptic cell adhesion mediated by binding of neuroligin 1 to α- and β-Neurexins. Neuron 48, 229–236.
Boucard, A.A., Maxeiner, S., Südhof, T.C., 2014. Latrophilins function as heterophilic cell-adhesion molecules by binding to teneurins. J. Biol. Chem. 289, 387–402.
Burbach, J.P.H., Meijer, D.H., 2019. Latrophilin's social protein network. Front. Neurosci. 13, 643.
Bushell, K.M., Söllner, C., Schuster-Boeckler, B., Bateman, A., Wright, G.J., 2008. Large-scale screening for novel low-affinity extracellular protein interactions. Genome Res. 18, 622–630.
Cain, S.A., et al., 2009. Defining elastic fiber interactions by molecular fishing. Mol. Cell. Proteom. 8, 2715–2732.
Causier, B., 2004. Studying the interactome with the yeast two-hybrid system and mass spectrometry. Mass Spectrom. Rev. 23, 350–367.
Chastney, M.R., Lawless, C., Humphries, M.J., 2020. Multiplexed proximity biotinylation coupled to mass spectrometry for defining integrin adhesion complexes. Curr. Protoc. Cell Biol. 88, e113.
Chataigner, L.M.P., et al., 2022. Structural insights into the contactin 1 – neurofascin 155 adhesion complex. Nat. Commun. 13, 6607.
Cheung, A., et al., 2022. Teneurin paralogues are able to localise synaptic sites driven by the intracellular domain and have the potential to form cis-heterodimers. Front. Neurosci. 16, 915149.
Cheung, A., Trevers, K.E., Reyes-Corral, M., Antinucci, P., Hindges, R., 2019. Expression and roles of teneurins in zebrafish. Front. Neurosci. 13, 158.
Dong, J.-M., et al., 2016. Proximity biotinylation provides insight into the molecular composition of focal adhesions at the nanometer scale. Sci. Signal. 9.
Ducrot, C., et al., 2025. High-affinity detection of biotinylated endogenous neuroligin-1 at excitatory and inhibitory synapses using a tagged knock-in mouse. Proc. Natl. Acad. Sci. 122, e2411669122.
Elegheert, J., et al., 2017. Structural mechanism for modulation of synaptic neuroligin-neurexin signaling by MDGA proteins. Neuron 95, 896–913.e10.
Gandawijaya, J., Bamford, R.A., Burbach, J.P.H., Oguro-Ando, A., 2021. Cell adhesion molecules involved in neurodevelopmental pathways implicated in 3p-deletion syndrome and autism spectrum disorder. Front. Cell. Neurosci. 14, 611379.
Gogou, C., et al., 2024. Alternative splicing controls teneurin-3 compact dimer formation for neuronal recognition. Nat. Commun. 15.
González-Calvo, I., et al., 2021. Sushi domain-containing protein 4 controls synaptic plasticity and motor learning. eLife 10.
Gonzalez-Lozano, M.A., et al., 2020. Stitching the synapse: cross-linking mass spectrometry into resolving synaptic protein interactions. Sci. Adv. 6, eaax5783.
Gorlewicz, A., Kaczmarek, L., 2018. Pathophysiology of trans-synaptic adhesion molecules: implications for epilepsy. Front. Cell Dev. Biol. 6, 119.
Guo, Z., et al., 2014. E-cadherin interactome complexity and robustness resolved by quantitative proteomics. Sci. Signal. 7.
Hillen, A.E.J., Burbach, J.P.H., Hol, E.M., 2018. Cell adhesion and matricellular support by astrocytes of the tripartite synapse. Prog. Neurobiol. 165–167, 66–86.
Hunyara, J.L., et al., 2023. Teneurin-3 regulates the generation of non-image-forming visual circuitry and responsiveness to light in the suprachiasmatic nucleus. PLOS Biol. 21, e3002412.
Kolberg, L., et al., 2023. g:Profiler—interoperable web service for functional enrichment analysis and gene identifier mapping (2023 update). Nucleic Acids Res. 51, W207–W212.
Li, J., et al., 2018. Structural basis for teneurin function in circuit-wiring: a toxin motif at the synapse. Cell 173, 735–748.e15.
Li, J., et al., 2020. Alternative splicing controls teneurin-latrophilin interaction and synapse specificity by a shape-shifting mechanism. Nat. Commun. 11, 2140.
Li, Q., Laumonnier, Y., Syrovets, T., Simmet, T., 2011. Yeast two-hybrid screening of proteins interacting with plasmin receptor subunit: C-terminal fragment of annexin A2. Acta Pharmacol. Sin. 32, 1411–1418.
Loh, K.H., et al., 2016. Proteomic analysis of unbounded cellular compartments: synaptic clefts. Cell 166, 1295–1307.e21.
Matzinger, M., Mechtler, K., 2021. Cleavable cross-linkers and mass spectrometry for the ultimate task of profiling protein–protein interaction networks *in Vivo*. J. Proteome Res. 20, 78–93.
Mayhew, M.W., et al., 2006. Identification of protein networks associated with the PAK1−βPIX−GIT1−paxillin signaling complex by mass spectrometry. J. Proteome Res. 5, 2417–2423.
Missler, M., Sudhof, T.C., Biederer, T., 2012. Synaptic cell adhesion. a005694–a005694 Cold Spring Harb. Perspect. Biol. 4. a005694–a005694.
Mohammed, H., Carroll, J.S., 2013. Approaches for assessing and discovering protein interactions in cancer. Mol. Cancer Res. 11, 1295–1302.
Mosca, T.J., 2015. On the Teneurin track: a new synaptic organization molecule emerges. Front. Cell. Neurosci. 9.
Orwick-Rydmark, M., Arnold, T., Linke, D., 2016. The use of detergents to purify membrane proteins. Curr. Protoc. Protein Sci. 84.
Parcerisas, A., et al., 2021. New partners identified by mass spectrometry assay reveal functions of NCAM2 in neural cytoskeleton organization. Int. J. Mol. Sci. 22, 7404.
Pederick, D.T., et al., 2021. Reciprocal repulsions instruct the precise assembly of parallel hippocampal networks. Science 372, 1068–1073.
Piersimoni, L., Kastritis, P.L., Arlt, C., Sinz, A., 2022. Cross-linking mass spectrometry for investigating protein conformations and protein–protein interactions—A method for all seasons. Chem. Rev. 122, 7500–7531.
Poulopoulos, A., et al., 2012. Homodimerization and isoform-specific heterodimerization of neuroligins. Biochem. J. 446, 321–330.
Ranaivoson, F.M., et al., 2019. A proteomic screen of neuronal cell-surface molecules reveals IgLONs as structurally conserved interaction modules at the synapse. Structure 27, 893–906.e9.
Rice, H.C., et al., 2019. Secreted amyloid-β precursor protein functions as a $GABA_B$ R1a ligand to modulate synaptic transmission. Science 363.
Roux, K.J., Kim, D.I., Raida, M., Burke, B., 2012. A promiscuous biotin ligase fusion protein identifies proximal and interacting proteins in mammalian cells. J. Cell Biol. 196, 801–810.
Roy, A., 2015. Membrane Preparation and Solubilization. In: in Methods in Enzymology, 557. Elsevier, pp. 45–56.
Sando, R., Jiang, X., Südhof, T.C., 2019. Latrophilin GPCRs direct synapse specificity by coincident binding of FLRTs and teneurins. Science 363, eaav7969.
Savas, J.N., et al., 2014. Ecto-Fc MS identifies ligand-receptor interactions through extracellular domain Fc fusion protein baits and shotgun proteomic analysis. Nat. Protoc. 9, 2061–2074.
Savas, J.N., et al., 2015. The sorting receptor SorCS1 regulates trafficking of neurexin and AMPA receptors. Neuron 87, 764–780.
Schöler, J., Ferralli, J., Thiry, S., Chiquet-Ehrismann, R., 2015. The intracellular domain of Teneurin-1 induces the activity of microphthalmia-associated transcription factor (MITF) by binding to transcriptional repressor HINT1. J. Biol. Chem. 290, 8154–8165.
Silva, J.-P., et al., 2011. Latrophilin 1 and its endogenous ligand Lasso/teneurin-2 form a high-affinity transsynaptic receptor pair with signaling capabilities. Proc. Natl. Acad. Sci. 108, 12113–12118.

The Integrin Interactome : *Methods and Protocols*. vol. 2217 (Springer US, New York, NY, 2021).
del Toro, D., et al., 2020b. Structural basis of teneurin-latrophilin interaction in repulsive guidance of migrating neurons. Cell 180, 323–339.e19.
Tran, H., Sawatari, A., Leamey, C.A., 2015. The glycoprotein Ten-m3 mediates topography and patterning of thalamostriatal projections from the parafascicular nucleus in mice. Eur. J. Neurosci. 41, 55–68.
Tyanova, S., et al., 2016. The Perseus computational platform for comprehensive analysis of (prote)omics data. Nat. Methods 13, 731–740.
Välikangas, T., Suomi, T., Elo, L.L., 2016. A systematic evaluation of normalization methods in quantitative label-free proteomics. Brief. Bioinform., bbw095 https://doi.org/10.1093/bib/bbw095.
Van Itallie, C.M., et al., 2013. Biotin ligase tagging identifies proteins proximal to E-cadherin, including lipoma preferred partner, a regulator of epithelial cell-cell and cell-substrate adhesion. J. Cell Sci., jcs.140475 https://doi.org/10.1242/jcs.140475.
Visser, J.J., et al., 2015. An extracellular biochemical screen reveals that FLRTs and Unc5s mediate neuronal subtype recognition in the retina. eLife 4, e08149.
Wojtowicz, W.M., et al., 2020. A human IgSF cell-surface interactome reveals a complex network of protein-protein interactions. e17 Cell 182, 1027–1043. e17.
Xu, C., et al., 2024. Molecular and cellular mechanisms of teneurin signaling in synaptic partner matching. Cell 187, 5081–5101.e19.
Young, T.R., Leamey, C.A., 2009. Teneurins: important regulators of neural circuitry. Int. J. Biochem. Cell Biol. 41, 990–993.
Zhang, Y., et al., 2019. Rapid identification of protein-protein interactions in plants. Curr. Protoc. Plant Biol. 4, e20099.